Inverse scattering problems with multi-frequencies

Topical Review

Inverse scattering problems with multi-frequencies

Gang Bao[1,5]**, Peijun Li**[2]**, Junshan Lin**[3] **and Faouzi Triki**[4]

[1] Department of Mathematics, Zhejiang University, Hangzhou, 310027, People's Republic of China
[2] Department of Mathematics, Purdue University, West Lafayette, IN 47907, USA
[3] Department of Mathematics and Statistics, Auburn University, Auburn, AL 36849, USA
[4] Laboratoire Jean Kuntzmann, Université Joseph Fourier, BP 53, F-38041 Grenoble Cedex 9, France

E-mail: baog@zju.edu.cn, lipeijun@math.purdue.edu, jzl0097@auburn.edu and faouzi.triki@imag.fr

CrossMark

Abstract

This paper is concerned with computational approaches and mathematical analysis for solving inverse scattering problems in the frequency domain. The problems arise in a diverse set of scientific areas with significant industrial, medical, and military applications. In addition to nonlinearity, there are two common difficulties associated with the inverse problems: ill-posedness and limited resolution (diffraction limit). Due to the diffraction limit, for a given frequency, only a low spatial frequency part of the desired parameter can be observed from measurements in the far field. The main idea developed here is that if the reconstruction is restricted to only the observable part, then the inversion will become stable. The challenging task is how to design stable numerical methods for solving these inverse scattering problems inspired by the diffraction limit. Recently, novel recursive linearization based algorithms have been presented in an attempt to answer the above question. These methods require multi-frequency scattering data and proceed via a continuation procedure with respect to the frequency from low to high. The objective of this paper is to give a brief review of these methods, their error estimates, and the related mathematical analysis. More attention is paid to the inverse medium and inverse source problems. Numerical experiments are included to illustrate the effectiveness of these methods.

Keywords: inverse scattering, multiple frequency, diffraction limit

---

[5] Author to whom any correspondence should be addressed

(Some figures may appear in colour only in the online journal)

1. Introduction

Scattering theory is concerned with the effect that a scatterer has on an incident field [87]. If the total field is viewed as the sum of an incident field and a scattered field, the direct scattering problems are to determine the scattered field from the incident field and the differential equations governing the wave motion; the inverse scattering problems are to determine the nature of the scatterer, such as location, geometry, or material property, from knowledge of the scattered field [50, 53, 54, 89, 92]. These problems have played important roles in diverse scientific areas such as radar and sonar (e.g., stealth aircraft design and submarine detection), geophysical exploration (e.g., oil and gas exploration), medical imaging (e.g., breast cancer detection), near-field optical microscopy (e.g., imaging of small scale biological samples), and nano-optics (e.g., design and fabrication of nano-scale optical elements).

In recent decades, the growth of computational capability and the development of fast algorithms have transformed the methodology for scientific investigation and industrial applications in the field of scattering theory. Reciprocally, the practical applications and scientific developments have driven the need for more sophisticated mathematical models and numerical algorithms to describe the scattering of complicated structures, and to accurately compute acoustic and electromagnetic fields and thus to predict the performance of a given structure, as well as to carry out optimal design of new structures. This paper is not intended to be a general survey of the inverse scattering problems. It is designed to be an introduction of the state of the art on computational approaches and mathematical analysis for solving the inverse scattering problems with multi-frequencies.

Due to lack of stability, the inverse scattering problems are severely ill-posed at a fixed frequency [70]. Small variations in the measured data can lead to large errors in the reconstructions, unless appropriate regularization methods are used to recover the information about the solution as stably as possible [63]. Interestingly, the Lipschitz stability results were obtained in [33, 34, 97, 98] for the time-domain acoustic wave equation which is equivalent to availability of the data corresponding to all frequencies. They motivate the intrinsic advantage of making use of multi-frequency data to gain increased stability for the time-harmonic scattering problems. According to the Heisenberg uncertainty principle, there is a resolution limit to the sharpness of details that can be observed by conventional optical microscopy, one half the wavelength, referred to as the diffraction limit [55, 56, 67, 100]. The diffraction limit provides a limit on the accuracy of the reconstruction for a given wavelength. To improve the resolution, it is desirable to use an incident field with a shorter wavelength or a higher frequency to illuminate the scatterer. However, it presents challenging mathematical and computational questions to realize this principle due to the nature of the underlying inverse problems.

Computational methods can be classified into two categories for solving the inverse scattering problems: nonlinear optimization based iterative methods [1, 36, 48, 61, 73, 75, 84–86, 90, 91, 94] and imaging based direct methods [37, 46, 47, 51, 52, 64, 68, 69, 76–80, 82, 83, 93]. The former are known as quantitative methods, that aim at recovering unknown functions which represent the scatterer. Although the methods are physically motivated with useful mathematical properties, they are computationally intensive since a sequence of direct and adjoint scattering problems need to be solved at iterations. Recently, this computation obstacle seems to be resolved with the ever-
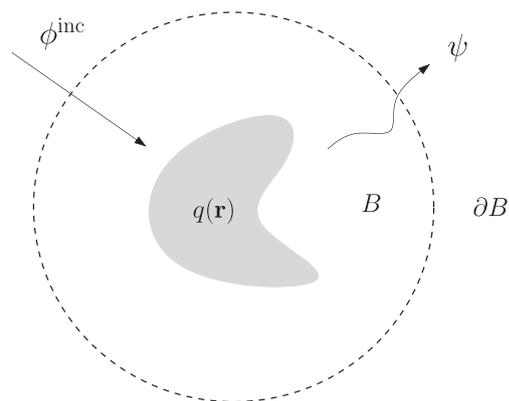
Figure 1. The inverse medium problem geometry. A plane wave ϕ^{inc} is incident on the scatterer, which is represented by the function q with a compact support contained in the ball B.

increasing of computing powers and the development of fast algorithms. The latter are called qualitative methods that attempt to visualize the scatterer by highlighting its boundary with designed imaging functions. Attractively, no direct solvers are needed, but they are not as accurate as those quantitative methods and might be time-consuming when evaluating the imaging functions over the whole domain particularly for three-dimensional problems. In addition, very little is known about the stability of the direct imaging methods.

The goal of this paper is to present the stable recursive linearization method (RLM) for solving quantitatively the inverse scattering problems with increased resolution. Specifically, we consider two representative examples among the inverse scattering problems: the non-linear inverse medium problem (IMP) and the linear inverse source problem (ISP). The method works equally well for many other inverse scattering problems such as the inverse obstacle scattering problem [24, 95] and the inverse surface scattering problem [22, 49]. Using the scalar model of the two-dimensional Helmholtz equation, we describe how the method proceeds via a continuation procedure with respect to the wavenumber for solving both the IMP and the ISP. The RLM actually takes a much simpler version when applying to the ISP since no linearization is needed. To validate the method mathematically, we show an error estimate for the IMP and a stability result for the ISP. Numerical examples are also reported to illustrate the effectiveness of the proposed method.

The outline of this paper is as follows. In section 2, the IMP is introduced; the variational problem is studied for the direct scattering; an energy estimate is given to provide a criterion for the weak scattering; the RLM is presented to solve the IMP. Section 3 is devoted to the ISP. The results of uniqueness and stability are given; a simpler version of the RLM is presented for solving the ISP. The paper is concluded with some general remarks and directions for future research in section 4. Throughout the paper, $a \lesssim b$ stands for $a \leqslant Cb$, where C is a positive constant, whose precise value is not required but should be always clear from the context.

2. Inverse medium problem

In this section, we consider the IMP, which is to reconstruct the inhomogeneous medium from the boundary measurement of the scattered field surrounding it.

2.1. A model problem

As seen in figure 1, we consider the two-dimensional Helmholtz equation

$$\Delta\phi + \kappa^2(1 + q)\phi = 0 \quad \text{in } \mathbb{R}^2, \tag{2.1}$$

where ϕ is the total field, $\kappa > 0$ is the wavenumber, and $q(\mathbf{r})$ is a real function known as the scatterer representing the inhomogeneous medium. We assume that the scatterer has a compact support contained in the ball $B = \{\mathbf{r} \in \mathbb{R}^2 : |\mathbf{r}| < R\}$ with boundary $\partial B = \{\mathbf{r} \in \mathbb{R}^2 : |\mathbf{r}| = R\}$, and satisfies $-1 < q_{min} \leqslant q \leqslant q_{max} < \infty$, where q_{min} and q_{max} are two constants.

The scatterer is illuminated by a plane incident field

$$\phi^{inc}(\mathbf{r}) = e^{i\kappa\mathbf{r}\cdot\mathbf{d}}, \tag{2.2}$$

where $\mathbf{d} = (\cos\theta, \sin\theta) \in \mathbb{S}^1 = \{\mathbf{r} \in \mathbb{R}^2 : |\mathbf{r}| = 1\}$ is the incident direction and $\theta \in (0, 2\pi)$ is the incident angle. Evidently, the incident field satisfies

$$\Delta\phi^{inc} + \kappa^2\phi^{inc} = 0 \quad \text{in } \mathbb{R}^2. \tag{2.3}$$

The total field ϕ consists of the incident field ϕ^{inc} and the scattered field ψ:

$$\phi = \phi^{inc} + \psi. \tag{2.4}$$

It follows from (2.1), (2.3) and (2.4) that the scattered field satisfies

$$\Delta\psi + \kappa^2(1 + q)\psi = -\kappa^2 q\phi^{inc} \quad \text{in } \mathbb{R}^2. \tag{2.5}$$

The scattered field is required to satisfy the Sommerfeld radiation condition:

$$\partial_r\psi - i\kappa\psi = o\left(r^{-1/2}\right) \quad \text{as } r = |\mathbf{r}| \to \infty. \tag{2.6}$$

Given the incident field ϕ^{inc}, the direct problem is to determine the scattered field ψ for the known scatterer q. Based on the Lax–Milgram theorem and the Fredholm alternative theorem, the direct problem can be shown to have a unique weak solution for all wavenumbers. An energy estimate is given for the scatterered field, which provides a criterion for the weak scattering. Furthermore, properties on the continuity and Fréchet differentiability of the nonlinear scattering map are examined. The IMP is to determine q from the boundary measurement of the scattered field ψ on ∂B, for the given incident field ϕ^{inc}.

The IMP arises naturally in diverse applications such as radar, sonar, geophysical exploration, medical imaging, and nondestructive testing [50]. In addition to being highly nonlinear, there are two other major difficulties associated with the inverse problem: the ill-posedness (unstable with respect to measurement errors) and the presence of many local minima (a common issue in minimizing nonlinear functions). A number of algorithms have been proposed for numerical solutions of this inverse problem, e.g., [38–42, 60, 66, 74, 99, 101, 102]. Classical iterative optimization methods offer fast local convergence but often fail to compute the global minimizers because of multiple local minima. Another issue is the ill-posedness, i.e., infinitesimal noise in the measured data may give rise to a large error in the computed solution. It is well known that the ill-posedness of the inverse scattering problem decreases as the frequency increases [3, 32]. However, at high frequencies, the nonlinear equation becomes extremely oscillatory and possesses many more local minima. A challenge for solving this problem is to develop a solution method that takes advantages of the regularity of the problem for high frequencies without being undermined by local minima.

To overcome the difficulties, a RLM was proposed in [43–45] for solving the IMP of the two-dimensional Helmholtz equation. Based on the Riccati equations for the scattering matrices, the method requires full aperture data and needs to solve a sensitivity matrix

equation at each iteration. Due to the high computational cost, it is numerically difficult to extend the method to the three-dimensional problems. Recently, we have developed new and more efficient RLMs for solving the two-dimensional Helmholtz equation and the three-dimensional Maxwell equations for both full and limited aperture data by direclty using the differential equation formulation [14–17, 20, 21, 23, 28, 31]. In the case of a fixed frequency, a novel RLM has also been developed by making use of the evanescent waves [18, 19]. Direct imaging techniques have been explored to replace the weak scattering for generating the initial guesses in [13, 24]. More recently, a hybrid method has been developed for solving the IMP with a stochastic source by combining the RLM and the Wiener chaos expansion [12]. We refer readers to [30] for the mathematical analysis of the general RLMs for solving the IMP with multi-frequency measurements.

In this section, for clarity of exposition, we present the RLM in the context of the IMP. The applications of RLM to the three-dimensional Maxwell's equations and inverse surface scattering problems impose additional challenging technical difficulties, but the main idea remains the same. The method, obtained by a continuation procedure on the wavenumber, requires multi-frequency scattering data. At each wavenumber, it determines a forward model which produces the prescribed scattering data. At a low wavenumber, the scattered field is weak. Consequently, the nonlinear equation becomes essentially linear, known as the Born approximation. It first solves this nearly linear equation at the lowest frequency to obtain low-frequency modes of the true scatterer. The approximation is then used to linearize the non-linear equation at the next higher wavenumber to produce a better approximation which contains more modes of the true scatterer. This process is continued until a sufficiently high wavenumber where the dominant modes of the scatterer are essentially recovered. The underlying physics which permits the successive recovery is the Heisenberg uncertainty principle: it is increasingly difficult to determine features of the scatterer as its size becomes decreasingly smaller than a half of a wavelength.

2.2. Variational problem

To describe the boundary value problem and derive its variational formulation, we introduce some function spaces. Denote by $L^2(B)$ and $L^\infty(B)$ the spaces of square integrable functions and bounded functions in B, respectively. Let $H^s(B)$ and $H^s(\partial B)$ be the standard Sobolev spaces equipped with the norms $\| \cdot \|_{s,B}$ and $\| \cdot \|_{s,\partial B}$. The dual space of $H^s(\partial B)$ is $H^{-s}(\partial B)$ with respect to the scalar product in $L^2(\partial B)$ defined by $\langle \cdot, \cdot \rangle$.

In the domain $\mathbb{R}^2 \backslash \bar{B}$, the solution of (2.5) can be written under the polar coordinates as follows:

$$\psi(r, \theta) = \sum_{n \in \mathbb{Z}} \frac{H_n^{(1)}(\kappa r)}{H_n^{(1)}(\kappa R)} \hat{\psi}_n e^{in\theta}, \tag{2.7}$$

where $H_n^{(1)}$ is the Hankel function of the first kind with order n and

$$\hat{\psi}_n = (2\pi)^{-1} \int_0^{2\pi} \psi(R, \theta) e^{-in\theta} d\theta.$$

Let $\mathscr{B} : H^{1/2}(\partial B) \to H^{-1/2}(\partial B)$ be the Dirichlet-to-Neumann (DtN) operator defined as follows: for any $\psi \in H^{1/2}(\partial B)$,

$$(\mathscr{B}\psi)(R, \theta) = \kappa \sum_{n \in \mathbb{Z}} \frac{H_n^{(1)'}(\kappa R)}{H_n^{(1)}(\kappa R)} \hat{\psi}_n e^{in\theta}. \tag{2.8}$$

Using the DtN operator, the solution in (2.7) satisfies the following transparent boundary condition

$$\partial_{\mathbf{n}}\psi = \mathscr{B}\psi \quad \text{on } \partial B, \tag{2.9}$$

where $\mathbf{n}$ is the unit outward normal on ∂B.

To state the variational problem, we introduce the sesquilinear form $a : H^1(B) \times H^1(B) \to \mathbb{C}$

$$a(\psi, \varphi) = \int_B \nabla\psi \cdot \nabla\bar{\varphi}\mathrm{d}\mathbf{r} - \kappa^2 \int_B (1 + q)\psi\bar{\varphi}\mathrm{d}\mathbf{r} - \langle \mathscr{B}\psi, \varphi \rangle, \tag{2.10}$$

where the bar denotes the complex conjugate. The direct problem (2.5), (2.9) is equivalent to the following variational problem: find $\psi \in H^1(B)$ such that

$$a(\psi, \varphi) = \kappa^2 \int_B q\phi^{\mathrm{inc}}\bar{\varphi}\mathrm{d}\mathbf{r} \quad \text{for all } \varphi \in H^1(B). \tag{2.11}$$

For a given scatterer q and an incident field ϕ^{inc}, we define the map $\mathscr{F}(q, \phi^{\mathrm{inc}}, \kappa)$ by $\psi = \mathscr{F}(q, \phi^{\mathrm{inc}}, \kappa)$, where ψ is the solution of the variational problem (2.11) at the wavenumber κ. It is easily seen that the map $\mathscr{F}(q, \phi^{\mathrm{inc}}, \kappa)$ is linear with respect to ϕ^{inc} but is nonlinear with respect to q. Hence, we may denote $\mathscr{F}(q, \phi^{\mathrm{inc}}, \kappa)$ by $\mathscr{F}(q, \kappa)\phi^{\mathrm{inc}}$.

Concerning the map $\mathscr{F}(q, \kappa)$, we have the following regularity results, which include the well-posedness of the variational problem (2.11) and energy estimates for the solution. All the proofs may be given by following step by step in [18]. Hence we omit them here.

Theorem 2.1. *There exists a small $\kappa_{\min} > 0$ depending on $q_{\max}$ such that if $\kappa \leqslant \kappa_{\min}$, the variational problem (2.11) has a unique weak solution in $H^1(B)$ and $\mathscr{F}(q, \kappa)$ is a bounded linear operator from $L^2(B)$ to $H^1(B)$ satisfying*

$$\| \mathscr{F}(q, \kappa)\phi^{\mathrm{inc}} \|_{1,B} \lesssim \kappa^2 \| \phi^{\mathrm{inc}} \|_{0,B}.$$

The energy estimate in theorem 2.1 provides a criterion for the weak scattering: the scattered field ψ is weak for a sufficiently small wavenumber κ.

For a general wavenumber $\kappa > 0$, the well-posedness of the variational problem (2.11) follows from the Fredholm alternative. However, the constant depends on the wavenumber and $q_{\min}$, $q_{\max}$ in the energy estimate.

Theorem 2.2. *The variational problem (2.11) has a unique weak solution for all $\kappa > 0$ and $\mathscr{F}(q, \kappa)$ is a linear bounded operator from $L^2(B)$ to $H^1(B)$ satisfying*

$$\| \mathscr{F}(q, \kappa)\phi^{\mathrm{inc}} \|_{1,B} \lesssim \| \phi^{\mathrm{inc}} \|_{0,B}.$$

Let $\mathscr{T}$ be the trace operator for the boundary ∂B. By the trace theorem, $\mathscr{T}$ is a bounded linear operator from $H^1(B)$ onto $H^{1/2}(\partial B)$. We can now define the scattering map $\mathscr{S}(q, \kappa) = (\mathscr{T} \circ \mathscr{F})(q, \kappa)$.

Next we consider the Fréchet differentiability of the scattering operator. Recall that $\mathscr{S}(q, \kappa)$ is nonlinear with respect to q. Formally, by using the first-order perturbation theory, we may obtain the linearized scattering problem (2.5), (2.9) with respect to a reference scatterer q:

$$\begin{cases} \Delta\delta\psi + \kappa^2(1 + q)\delta\psi = -\kappa^2\delta q\big(\phi^{\text{inc}} + \psi\big) & \text{in } B, \\ \partial_{\mathbf{n}}\delta\psi = \mathscr{B}\delta\psi & \text{on } \partial B, \end{cases} \tag{2.12}$$

where $\psi = \mathscr{F}(q, \kappa)\phi^{\text{inc}}$.

Define the formal linearization $\mathscr{L}(q, \kappa)$ of $\mathscr{F}(q, \kappa)$ by $\delta\psi = \mathscr{L}(q, \kappa)(\delta q, \phi^{\text{inc}})$, where $\delta\psi$ is the solution to the linearized problem (2.12). It can be shown that the linear operator $\mathscr{L}(q, \kappa)$ is bounded and continuous, and is the Fréchet derivative of the nonlinear operator $\mathscr{F}(q, \kappa)$. Hence, we may obtain the Fréchet differentiability of the scattering operator $\mathscr{S}(q, \kappa)$, which is useful for us to present the RLM.

Theorem 2.3. *The scattering operator $\mathscr{S}(q, \kappa)$ is Fréchet differentiable with respect to q and its Fréchet derivative is*

$$\mathscr{S}'(q, \kappa) = (\mathscr{T} \circ \mathscr{L})(q, \kappa).$$

The proof may be found in [18]. We refer to [10] and [4] for the regularity and stability analysis of the scattering operator for the two-dimensional Helmholtz equation and the three-dimensional Maxwell equation, respectively.

2.3. Born approximation

To initialize the RLM, an initial guess is needed and derived from the Born approximation.

Rewriting (2.5) as

$$\Delta\psi + \kappa^2\psi = -\kappa^2 q\big(\phi^{\text{inc}} + \psi\big). \tag{2.13}$$

It follows from the energy estimate in theorem (2.1) that the scattered field ψ is weak for sufficiently small wavenumber. Dropping the scattered field in the right-hand side of (2.13), we consider the Born approximation:

$$\begin{cases} \Delta\psi_B + \kappa^2\psi_B = -\kappa^2 q\phi^{\text{inc}} & \text{in } B, \\ \partial_{\mathbf{n}}\psi_B = \mathscr{B}\psi_B & \text{on } \partial B. \end{cases} \tag{2.14}$$

It is shown in [12] that there exists a small $\kappa_{\min} > 0$ such that if $\kappa \leqslant \kappa_{\min}$ it holds the following error estimate for the Born approximation of the scattered field:

$$\| \psi - \psi_B \|_{1,B} \lesssim \kappa^4 \| \phi^{\text{inc}} \|_{0,B},$$

which implies that ψ_B is a good approximation to the scattered field ψ for sufficiently small κ.

If the scattering data ψ is available for the full aperture on the whole ∂B, the field ψ_B of (2.14), as a good approximation to ψ, can be viewed as a known quantity on ∂B. The plane waves turn out to be useful to obtain an initial guess.

Consider an auxiliary function

$$\psi^{\text{inc}}(\mathbf{r}) = e^{i\kappa\mathbf{r}\cdot\mathbf{p}}, \tag{2.15}$$

where $\mathbf{p} = (\cos\beta, \sin\beta) \in \mathbb{S}^1$, $\beta \in [0, 2\pi)$. Obviously, the auxiliary function represents propagating plane waves and satisfies the Helmholtz equation

$$\Delta\psi^{\text{inc}} + \kappa^2\psi^{\text{inc}} = 0 \quad \text{in } \mathbb{R}^2.$$

Multiplying (2.14) by ψ^{inc} and integrating in B on both sides, we have

$$\int_B \Delta \psi_B\, \psi^{\mathrm{inc}} \mathrm{d}\mathbf{r} + \kappa^2 \int_B \psi_B\, \psi^{\mathrm{inc}} \mathrm{d}\mathbf{r} = -\kappa^2 \int_B q\phi^{\mathrm{inc}}\psi^{\mathrm{inc}}\mathrm{d}\mathbf{r}.$$

Integration by parts yields

$$\int_{\partial B} \left(\psi^{\mathrm{inc}}\partial_{\mathbf{n}}\psi_B - \psi_B \partial_{\mathbf{n}}\psi^{\mathrm{inc}} \right)\mathrm{d}\mathbf{r} = -\kappa^2 \int_B q\phi^{\mathrm{inc}}\psi^{\mathrm{inc}}\mathrm{d}\mathbf{r}.$$

Using the DtN operator (2.9), we may obtain a linear integral equation for the scatterer q:

$$\int_B q\phi^{\mathrm{inc}}\psi^{\mathrm{inc}}\mathrm{d}\mathbf{r} = \kappa^{-2} \int_{\partial B} \left(\psi_B \partial_{\mathbf{n}}\psi^{\mathrm{inc}} - \psi^{\mathrm{inc}}\mathscr{B}\psi_B \right)\mathrm{d}s,$$

where the right-hand side of the above equation is known since ψ_B is available on ∂B. Noting (2.2) and (2.15), we obtain

$$\int_B q(\mathbf{r})\mathrm{e}^{i\kappa\mathbf{r}\cdot(\mathbf{d}+\mathbf{p})}\mathrm{d}\mathbf{r} = \kappa^{-2} \int_{\partial B} \left(\psi_B \partial_{\mathbf{n}}\psi^{\mathrm{inc}} - \psi^{\mathrm{inc}}\mathscr{B}\psi_B \right)\mathrm{d}s,$$

which gives the Fourier transform of q:

$$\hat{q}(\xi) = \kappa^{-2} \int_{\partial B} \left(\psi_B \partial_n \psi^{\mathrm{inc}} - \psi^{\mathrm{inc}}\mathscr{B}\psi_B \right)\mathrm{d}s. \tag{2.16}$$

Here $\xi = \kappa(\mathbf{d}+\mathbf{p})$ satisfies $|\xi| \leqslant 2\kappa$. Thus only the low Fourier modes of $\hat{q}(\xi)$ in the ball $\{\xi : |\xi| \leqslant 2\kappa\}$ can be determined since κ is small for the Born approximation. The scattering data with the higher wavenumber must be used in order to recover more Fourier modes of the true scatterer.

2.4. Recursive linearization

Let $\kappa_{\min} > 0$ be the constant defined in theorem 2.1 and $\kappa_{\max}$ be a constant which is much larger than $\kappa_{\min}$. Assume that the scattering data ψ is available over a range of wavenumbers $\kappa \in [\kappa_{\min}, \kappa_{\max}]$, which may be divided into $\kappa_{\min} = \kappa_0 < \kappa_1 < \cdots < \kappa_{N-1} < \kappa_N = \kappa_{\max}$. We now describe a procedure that recursively determines a better approximation q_j at the wavenumber $\kappa = \kappa_j$ for $j = 1, 2,...,N$ with $\kappa_1 < \kappa_2 < \cdots < \kappa_N$ in a increasing manner.

Suppose now that an approximation of the scatterer q_{j-1} has been recovered at the wavenumber κ_{j-1}. We wish to determine q_j, or equivalently, to determine the perturbation

$$\delta q_j = q_j - q_{j-1}. \tag{2.17}$$

For the recovered scatterer q_{j-1}, we solve at the wavenumber κ_j the direct problem

$$\begin{cases} \Delta\psi_j + \kappa_j^2\left(1 + q_{j-1}\right)\psi_j = -\kappa_j^2 q_{j-1}\phi^{\mathrm{inc}} & \text{in } B, \\ \partial_{\mathbf{n}}\psi_j = \mathscr{B}\psi_j & \text{on } \partial B. \end{cases} \tag{2.18}$$

For the scatterer q_j, we have

$$\begin{cases} \Delta\left(\psi_j + \delta\psi_j\right) + \kappa_j^2\left(1 + q_j\right)\left(\psi_j + \delta\psi_j\right) = -\kappa_j^2 q_j\phi^{\mathrm{inc}} & \text{in } B, \\ \partial_{\mathbf{n}}\left(\psi_j + \delta\psi_j\right) = \mathscr{B}\left(\psi_j + \delta\psi_j\right) & \text{on } \partial B. \end{cases} \tag{2.19}$$

Subtracting (2.18) from (2.19) and omitting the second-order smallness in δq_j and $\delta\psi_j$, we obtain

$$\begin{cases} \Delta\delta\psi_j + \kappa_j^2\big(1 + q_j\big)\delta\psi_j = -\kappa_j^2\delta q_j\big(\phi^{\mathrm{inc}} + \psi_j\big) & \text{in } B, \\ \qquad\qquad\qquad \partial_{\mathbf{n}}\delta\psi_j = \mathscr{B}\delta\psi_j & \text{on } \partial B. \end{cases} \tag{2.20}$$

For the scatterer q_j and the incident field ϕ^{inc}, we have from (2.19) that

$$\mathscr{F}(q_j,\ \kappa_j)\phi^{\mathrm{inc}} = \psi_j + \delta\psi_j,$$

Recall the scattering map

$$\mathscr{S}(q_j,\ \kappa_j)\phi^{\mathrm{inc}} = (\mathscr{T}\circ\mathscr{F})(q_j,\ \kappa_j)\phi^{\mathrm{inc}}.$$

By the definition of the trace operator, we have

$$\mathscr{S}(q_j,\ \kappa_j)\phi^{\mathrm{inc}} = \big(\psi_j + \delta\psi_j\big)|_{\partial B}.$$

Let $\mathscr{S}'(q_{j-1},\ \kappa_j)$ be the Fréchet derivative of $\mathscr{S}(q_j,\ \kappa_j)$ and denote the residual operator

$$\mathscr{R}(q_{j-1},\ \kappa_j) = \delta\psi_j\,|_{\partial B}.$$

It follows from theorem 2.3 that

$$\mathscr{S}'(q_{j-1},\ \kappa_j)\delta q_j = \mathscr{R}(q_{j-1},\ \kappa_j) = \delta\psi_j\,|_{\partial B}. \tag{2.21}$$

We apply the Landweber iteration (see, [63]) to the above equation and obtain

$$\delta q_j = \alpha\Big(\big(\mathscr{S}'\big)^*\circ\mathscr{R}\Big)(q_{j-1},\ \kappa_j), \tag{2.22}$$

where $\alpha > 0$ is a positive relaxation parameter and $(\mathscr{S}')^*$ is the adjoint operator of $\mathscr{S}'$.

We consider the following adjoint problem to efficiently compute $((\mathscr{S}')^*\circ\mathscr{R})(q_{j-1},\ \kappa_j)$:

$$\begin{cases} \Delta\varphi_j + \kappa_j^2(1 + q)\varphi_j = 0 & \text{in } B, \\ \partial_{\mathbf{n}}\varphi_j - \mathscr{B}^*\varphi_j = \mathscr{R}(q_{j-1},\ \kappa_j) & \text{on } \partial B, \end{cases} \tag{2.23}$$

where $\mathscr{B}^*$ is the adjoint operator of $\mathscr{B}$ and is defined by

$$\big(\mathscr{B}^*\psi\big)(R,\ \theta) = \kappa\sum_{n\in\mathbb{Z}}\frac{\bar{H}_n^{(1)'}(\kappa R)}{\bar{H}_n^{(1)}(\kappa R)}\hat{\psi}_n\mathrm{e}^{\mathrm{i}n\theta},\quad \hat{\psi}_n = (2\pi)^{-1}\int_0^{2\pi}\psi(R,\ \theta)\mathrm{e}^{-\mathrm{i}n\theta}\mathrm{d}\theta.$$

Multiplying (2.20) with the complex conjugate of φ_j and integrating over B on both sides, we obtain

$$\int_B \Delta\delta\psi_j\bar{\varphi}_j\mathrm{d}\mathbf{r} + \kappa_j^2\int_B\big(1 + q_j\big)\delta\psi_j\bar{\varphi}_j\mathrm{d}\mathbf{r} = -\kappa_j^2\int_B\delta q_j\big(\phi^{\mathrm{inc}} + \psi_j\big)\bar{\varphi}_j\mathrm{d}\mathbf{r}.$$

It follows from Green's formula and the adjoint problem (2.23) that we have

$$\int_{\partial B}\delta\psi_j\bar{\mathscr{R}}(q_{j-1},\ \kappa_j)\mathrm{d}r = \kappa_j^2\int_B\delta q_j\big(\phi^{\mathrm{inc}} + \psi_j\big)\bar{\varphi}_j\mathrm{d}\mathbf{r}.$$

It follows from (2.21) that

$$\Big\langle\mathscr{S}'(q_{j-1},\ \kappa_j)\delta q_j,\ \mathscr{R}(q_{j-1},\ \kappa_j)\Big\rangle = \kappa_j^2\int_B\delta q_j\big(\phi^{\mathrm{inc}} + \psi_j\big)\bar{\varphi}_j\mathrm{d}\mathbf{r},$$

which implies

$$\int_B\delta q_j\Big(\big(\mathscr{S}'\big)^*\circ\mathscr{R}\Big)(q_{j-1},\ \kappa_j)\mathrm{d}\mathbf{r} = \kappa_j^2\int_B\delta q_j\big(\phi^{\mathrm{inc}} + \psi_j\big)\bar{\varphi}_j\mathrm{d}\mathbf{r}.$$

Since it hold for any δq_j, we have after combining (2.22) that

$$\delta q_j = \alpha \kappa_j^2 \left(\bar{\phi}^{\text{inc}} + \bar{\psi}_j \right) \varphi_j. \tag{2.24}$$

Thus for each iteration, we solve one direct problem (2.18) and one adjoint problem (2.23). Since the adjoint problem has a variational form similar to that of the direct problem, we need to compute essentially two direct problems at each step. Once the correction δq_j is available, q_j is updated by $q_{j-1} + \delta q_j$. The procedure is repeated for $j = 1, ..., N$.

2.5. Error estimate

At the wavenumber κ, consider the objective functional

$$\mathcal{J}(q) = \frac{1}{2} \int_{\partial B} |\mathscr{S}(q, \kappa) - \psi|^2 \mathrm{d}s + \frac{\gamma}{2} \int_B |\nabla q|^2 \mathrm{d}\mathbf{r},$$

where ψ is the scattering data on ∂B at the wavenumber κ and $\gamma > 0$ is the regularization parameter. Clearly, the objective functional consists of the cost functional and the regularization functional. The inverse medium scattering problem can formulated into the minimization problem:

$$\min \mathcal{J}(q).$$

The regularization term filters high frequency oscillations and stabilizes the minimization problem. The regularization parameter γ fixes the resolution. Here we take a usual L^2 regularization for an example by assuming a smooth scatterer function q. A total variation type regularization may be considered if q is a piecewise constant function.

To minimize the objective functional by a gradient method, it is required to compute the Fréchet derivative of the cost and regularization functionals. Denote the residual $\mathscr{R}(q, \kappa) = \mathscr{S}(q, \kappa) - \psi$. A simple calculation yields the derivative of the objective functional at q:

$$
\begin{aligned}
\mathcal{J}'(q)\delta q &= \mathrm{Re} \int_{\partial B} \mathscr{S}'(q, \kappa)\delta q \bar{\mathscr{R}}(q, \kappa)\mathrm{d}s + \gamma \int_B \Delta q \delta q \mathrm{d}\mathbf{r}, \\
&= \mathrm{Re}\langle \mathscr{S}'(q, \kappa)\delta q, \mathscr{R}(q, \kappa) \rangle + \int_B \delta q \gamma \Delta q \mathrm{d}\mathbf{r}, \\
&= \mathrm{Re} \int_B \delta q \left(\left(\mathscr{S}' \right)^* \circ \mathscr{R} \right)(q, \kappa)\mathrm{d}\mathbf{r} + \int_B \delta q \gamma \Delta q \mathrm{d}\mathbf{r}. \tag{2.25}
\end{aligned}
$$

Similarly, we may consider the following adjoint problem to efficiently compute $((\mathscr{S}')^* \circ R)(q, \kappa_j)$:

$$
\begin{cases}
\Delta \varphi + \kappa^2 (1 + q)\varphi = 0 & \text{in } B, \\
\partial_{\mathbf{n}} \varphi - \mathscr{B}^* \varphi = \mathscr{R}(q, \kappa) & \text{on } \partial B.
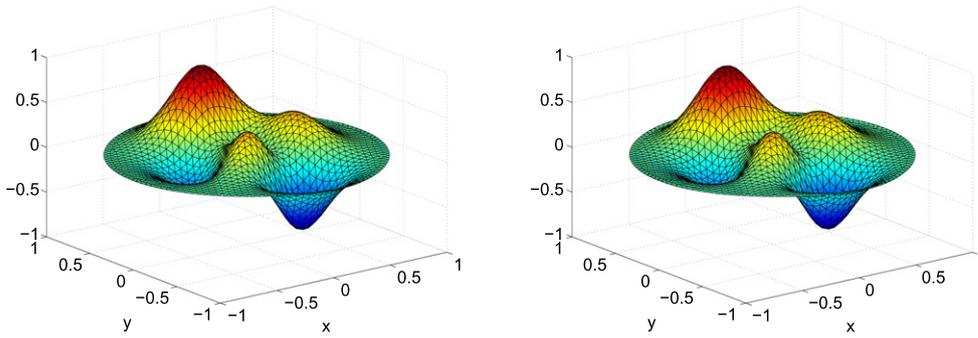\end{cases}
$$

Repeating the same step in the previous section, we derive that

$$\left(\left(\mathscr{S}' \right)^* \circ \mathscr{R} \right)(q, \kappa) = \kappa^2 \left(\bar{\phi}^{\text{inc}} + \bar{\psi} \right) \varphi, \tag{2.26}$$

where $\psi = \mathscr{S}(q, \kappa)$ is the solution of the direct problem with the scatterer q at the wavenumber κ.

Combining (2.25) and (2.26) yields the Fréchet derivative of the objective functional:

$$\mathcal{J}'(q) = \mathrm{Re} \left[\kappa^2 \left(\bar{\phi}^{\text{inc}} + \bar{\psi} \right) \varphi \right] + \gamma \Delta q. \tag{2.27}$$

Figure 2. The inverse medium scattering problem: (left) exact scatterer; (right) reconstructed scatterer.

Comparing (2.24) with (2.27), we derive the same Fréchet derivative from two different points of view: one is derived via operator equations and another is based on the optimization approach.

The following is the main result of the error estimate of the RLM for solving the inverse medium scattering problem. The proof may be found in [30].

Theorem 2.4. *Assume that the scattering data $\psi(\kappa)$ is available for $\kappa \in [\kappa_{\min}, \quad \kappa_{\max}]$. Let $\kappa_j = \kappa_{\min} + j(\kappa_{\max} - \kappa_{\min})/N$, $j = 0, 1, ..., N$ and $\tilde{q}(\kappa_j)$ is a q_j-minimum norm solution, i.e., among all solutions of $\mathscr{S}(q, \kappa_j) = \psi(\kappa_j)$, $\tilde{q}(\kappa_j)$ minimizes the distant to q_j for $0 \leqslant j \leqslant N$. There exist positive constants γ and N_0 such that if*

$$\| \tilde{q}(\kappa_0) - q_0 \|_{0,B} \lesssim \gamma,$$

then it holds for all $N \geqslant N_0$ that

$$\| \tilde{q}(\kappa_N) - q_N \|_{0,B} \lesssim \gamma^{-1/2} N^{-1}.$$

According to theorem 2.4, if the error of the initial guess at lowest wavenumber $\kappa_{\min}$ is of the order of γ (small positive regularization parameter), the algorithm converges linearly to the observable part of the true scatterer $\tilde{q}(\kappa_{\max})$. The convergence result may be interpreted as follows: if a good estimate of the first few Fourier modes of the scatterer at $\kappa_{\min}$ is available, then the algorithm will provide a good approximation of the observable part $\tilde{q}(\kappa_{\max})$ of the scatterer at a computational cost which is proportional to $\gamma^{-1/2}$. The derivation of the error between the true scatterer q and its observable part $\tilde{q}(\kappa_{\max})$ is strongly linked to the uniqueness, and particularly the stability of the inverse problem with increased wavenumber, which is open and remains for future work.

2.6. Numerical experiments

The scattering data is obtained by the numerical solution of the direct problem, which is implemented by using the finite element method with the perfectly matched layer technique. We present an example to illustrate the performance of the method.

Let

$$\tilde{q}(x, y) = 0.3(1 - x)^2 e^{-x^2-(y+1)^2} - \left(0.2x - x^3 - y^5\right)e^{-x^2-y^2} - 0.03e^{-(x+1)^2-y^2}$$
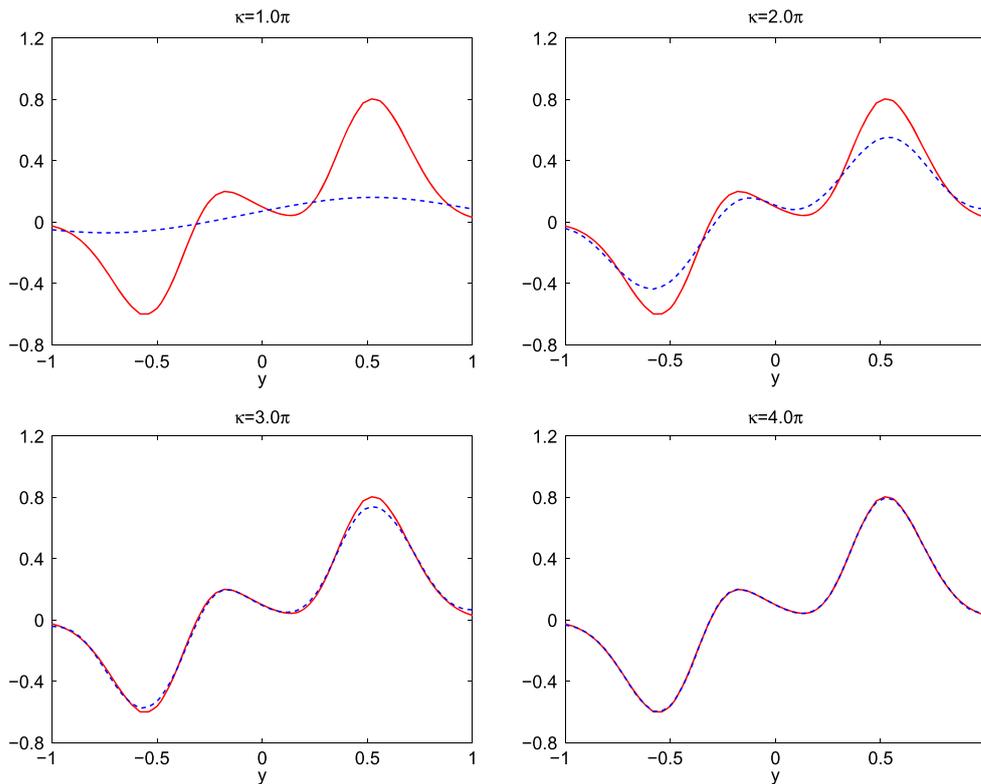
Figure 3. The reconstructed scatterer (dashed line) is plotted against the exact scatterer (solid line) for the cross-section $x = 0$.

and reconstruct a scatterer defined by

$$q(x, y) = \tilde{q}(3x, 3y)$$

inside the unit ball $B = \{\mathbf{r} \in \mathbb{R}^2 : |\mathbf{r}| < 1\}$, see figure 2 (left) for the surface plot of the exact scatterer function in the domain B. Eleven equally spaced wavenumbers are used in the construction, starting from the lowest wavenumber $\kappa_{\min} = 0.5\pi$ (corresponding to the wavelength $\lambda = 4.0$) and ending at the highest wavenumber $\kappa_{\max} = 4.0\pi$ (corresponding to the wavelength $\lambda = 0.5$). Denote by $\Delta\kappa = (\kappa_{\max} - \kappa_{\min})/7 = 0.5\pi$ the step size of the wavenumber; then the seven equally spaced wavenumbers are $\kappa_j = \kappa_{\min} + j\Delta\kappa, j = 0,..., 7$. The number of incident fields is taken as 20, which accounts for 20 Landweber iterations at each wavenumber. The relaxation parameter α is 0.01. The relative $L^2(B)$ error of reconstruction is listed in table 1 at eight wavenumbers; the error decreases from 9.49×10^{-1} to 1.41×10^{-2} as the wavenumber increases from $\kappa_0 = 0.5\pi$ to $\kappa_7 = 4.0\pi$. The reconstructed scatterer function is plotted in figure 2 (right), which is almost identical to the exact scatterer function from the plot. A cross-section reconstruction of the scatterer at $x = 0$ is shown against the exact scatterer at four different wavenumbers in figure 3. The convergence of the method is clearly shown as the wavenumber is increased.

To test the stability of the method, we reconstruct the scatterer with noisy data. Some relative random noise is added to the data, i.e., the scattering data takes

Table 1. Relative $L^2(B)$ error of reconstruction at different wavenumbers.

κ	κ_0	κ_1	κ_2	κ_3
e_2	9.49×10^{-1}	7.86×10^{-1}	4.91×10^{-1}	2.52×10^{-1}
κ	κ_4	κ_5	κ_6	κ_7
e_2	1.23×10^{-1}	5.49×10^{-2}	2.53×10^{-2}	1.41×10^{-2}

Table 2. Relative $L^2(B)$ error of reconstruction with noisy data.

σ	1%	3%	5%	7%	9%
e_2	1.44×10^{-2}	1.56×10^{-2}	1.80×10^{-2}	2.16×10^{-2}	2.55×10^{-2}

$$\psi \mid_{\partial B} := (1 + \sigma \mathrm{rand})\psi \mid_{\partial B}.$$

Here rand stands for uniformly distributed random numbers in $[-1, \ 1]$ and σ is the noise level parameter. Five tests are made here corresponding to the noise level added to the scattering data to $\sigma = 1\%, 3\%, 5\%, 7\%, 9\%$. The relative $L^2(B)$ error are listed in table 2, which shows that the method is stable with respect to the noise.

3. Inverse source problem

In this section, we consider the ISP that determines the unknown current density function from measurements of the radiated fields at multiple wavenumbers.

3.1. A model problem

Consider the two-dimensional Helmholtz equation

$$\Delta\psi + \kappa^2\psi = f \quad \text{in } \mathbb{R}^2, \tag{3.1}$$

where κ is the wavenumber, ψ is the radiated scalar field, and the source current density function $f(\mathbf{r})$ is assumed to have a compact support contained in $B = \{\mathrm{r} \in \mathbb{R}^2 : |\mathbf{r}| \leqslant R\}$. The radiated field ψ satisfies the Sommerfeld radiation condition:

$$\partial_r\psi - \mathrm{i}\kappa\psi = o\left(r^{-1/2}\right) \quad \text{as } r = |\mathbf{r}| \to \infty. \tag{3.2}$$

Since ψ depends on the wavenumber κ, we sometimes employ $\psi(\kappa, \mathbf{r})$ in place of $\psi(\mathbf{r})$ to emphasize the dependence on the wavenumber κ.

Similarly, in the domain $\mathbb{R}^2 \setminus \bar{B}$, the solution of (3.1) has a series expansion (2.7) in the polar coordinates. Using the DtN operator (2.8), the solution of (3.1) satisfies the transparent boundary condition

$$\partial_{\mathbf{n}}\psi = \mathscr{B}\psi \quad \text{on } \partial B, \tag{3.3}$$

where $\mathbf{n}$ is the unit outward normal on ∂B.

Given the source density function f, the direct problem is to determine the radiated field ψ. The ISP is to determine the source function f from the boundary measurement of the radiated field on the boundary ∂B, i.e., $\mathscr{T}\psi(\kappa, \mathbf{r})$, for all $\kappa \in (0, \ \bar{\kappa}]$, where $\mathscr{T}$ is the trace operator and $\bar{\kappa} > 0$ is a given constant.

The ISP has many significant applications in biomedical engineering and antenna synthesis. In medical application it is desired to use the measurement of the radiated electromagnetic field on the surface of the human brain to infer the abnormalities inside the brain [57]. In antenna synthesis, the ISP is to reconstruct the unknown current distribution along a linear antenna which produces the desired radiated field [7]. The problem also arises naturally in identification of pollutant in the environment [81].

The mathematical studies of the ISP for electromagnetism date back to [35], where the uniqueness of the problem was investigated at a fixed frequency. It is now well known that a source with an extended support cannot be uniquely determined from surface measurements at a fixed frequency due to the existence of infinitely many non-radiating fields [2, 58, 59, 65, 71, 72]. Therefore, in order to obtain a unique solution to the problem, additional constraints need to be imposed on the source. A usual choice is to find the source with a minimum energy norm. However, the difference between the minimum energy solution and the original source function could be significant. Another difficulty of the ISP at fixed frequency is brought by its inherited instability. This is due to exponential decay of the singular eigenvalues of the forward operator [25–27, 62]. For the special cases of reconstruction for point sources, we refer the readers to [5, 8, 9, 96] for studies of the unique identifiability and stability of the problem. If the source consists of dipoles only, numerical reconstruction based on algebraic formulations can be applied. More recently, an inverse random source scattering problem has been studied in [11, 57, 88], where the current source density function is modeled as a random function.

The use of the multiple frequency data for the ISP provides an approach to circumvent the difficulties of non-uniqueness and instability presented at a fixed frequency [29, 62]. Indeed, the results of uniqueness and stability can be established for the case of multiple frequency measurements. It can be shown that the inverse problem is uniquely solvable and is Lipschitz stable when the highest wavenumber exceeds a certain real number. The theoretical results shed a light on the stability estimate for more challenging nonlinear problems such as the IMP discussed in section 2. Computationally, we present a continuation procedure along the wavenumbers for solving the ISP. The method has the same spirit as the RLM, although the linearization step is not needed since the ISP is a linear problem.

3.2. Uniqueness and stability

Let $\xi \in \mathbb{R}^2$ such that $|\xi| = \kappa \in (0, \; \bar{\kappa}]$. Multiplying (3.1) by $e^{-i\xi \cdot r}$ and integrating over B, we obtain

$$\hat{f}(\xi) = \int_{\partial B} e^{-i\xi \cdot \mathbf{r}} \big[\partial_{\mathbf{n}} \psi(\kappa, \mathbf{r}) + i\xi \cdot \mathbf{n} \psi(\kappa, \mathbf{r}) \big],$$

which implies from the boundary condition (3.3) that

$$\hat{f}(\xi) = \int_{\partial B} e^{-i\xi \cdot \mathbf{r}} (\mathscr{B} + i\xi \cdot \mathbf{n}) \psi(\kappa, \mathbf{r}).$$

It is evident from the above formula that by collecting the measurements $\psi(\kappa, \mathbf{r})$ on a band of wavenumber in $(0, \; \bar{\kappa}]$, the Fourier transform of f on the frequency interval $(0, \; \bar{\kappa}]$ can be reconstructed directly. In addition, the following result indicates that this amount of information is sufficient to determine the source function f uniquely.

Theorem 3.1. *Let κ_j be a set of real numbers with an accumulation point. Then the measurements $\psi(\kappa_j, \mathbf{r})$ on ∂B determine uniquely the source function f.*

The next result is concerned with the stability estimates of the multi-frequency ISP. The readers are referred to [25] for the details of the proof.

Theorem 3.2. *Let $f \in C^1(B)$ with a compact support in B, and assume that*

$$\epsilon = \| \partial_{\mathbf{n}} \psi \|_{L^1([0, \, \bar{\kappa}] \times \, \partial B)} + \| \kappa \psi \|_{L^1([0, \, \bar{\kappa}] \times \, \partial B)} < 1$$

and

$$\| f \|_{C^1(B)} \leqslant M,$$

where M is a strictly positive constant. The following statements hold:

(i) *If $\bar{\kappa} \geqslant \epsilon^{-4} + 1$, then*

$$\| f \|_{C^0(B)} \lesssim \left[1 + M \left(1 + \frac{1}{\bar{\kappa}} \right) + \left(\frac{1}{\bar{\kappa}} \right)^{\frac{3}{2}} \right] \epsilon,$$

(ii) *If $\bar{\kappa} < \epsilon^{-4} + 1$, then*

$$\| f \|_{C^0(B)} \lesssim \left[1 + M \left(1 + \frac{1}{\bar{\kappa}} \right) \left(\left(\frac{1}{\bar{\kappa}} \right) + \left(\frac{1}{\bar{\kappa}} \right)^{\frac{1}{2}} \right)^{\frac{1}{6}} \right] \frac{1}{(-\ln \epsilon)^{\frac{1}{6}}}.$$

The result in theorem 3.2 shows clearly that if the source function f is compactly supported in B and the measurement $\psi(\kappa, \mathbf{r})$ is taken for $\kappa \in (0, \, \bar{\kappa}]$ with a noise ϵ, then the recovery of f is linearly and logarithmic stable with respect to the noise for large and small $\bar{\kappa}$, respectively. These theoritical stability results confirm the physical expectations on increasing the resolution by taking multi-frequency data.

3.3. Numerical experiments

It is assumed that the radiating fields ψ is measured over a range of wavenumbers $\kappa \in [\kappa_{\min}, \kappa_{\max}]$ on ∂B. Let $\mathscr{S}(\kappa)$ be the forward scattering operator which maps the source function f to the measurement ψ such that $\psi = \mathscr{S}(\kappa)f$. Similar to the inverse medium scattering, the numerical algorithm for ISP divides the wavenumber interval by setting $\kappa_{\min} = \kappa_0 < \kappa_1 < \cdots < \kappa_{N-1} < \kappa_N = \kappa_{\max}$, and adopts a continuation procedure along the wavenumber by recursively obtaining an approximation f_j at the wavenumber $\kappa = \kappa_j$ for $j = 0, 1, 2, ..., N$. We note that the ISP is linear, hence the linearization procedure as in the inverse medium scattering is not required. Instead, a straightforward Landweber iteration can applied as a regularization scheme at each fixed wavenumber. More precisely, suppose that an approximation of the source f_{j-1} has been recovered at the wavenumber κ_{j-1}, the steepest descent direction δf_j is chosen such that

$$\delta f_j = \mathscr{S}^*(\kappa_j) \left(\psi_j - \mathscr{S}(\kappa_j) f_{j-1} \right),$$

where $\mathscr{S}^*(\kappa_j)$ is the adjoint operator of $\mathscr{S}(\kappa_j)$, and ψ_j denotes the radiating field at κ_j. The reconstruction at κ_j is updated by the formula $f_j = f_{j-1} + \alpha_j \delta f_j$, where α_j is a suitable step length. This downhill process is done iteratively at $\kappa = \kappa_j$ until the solution f_j reaches the admissible accuracy.
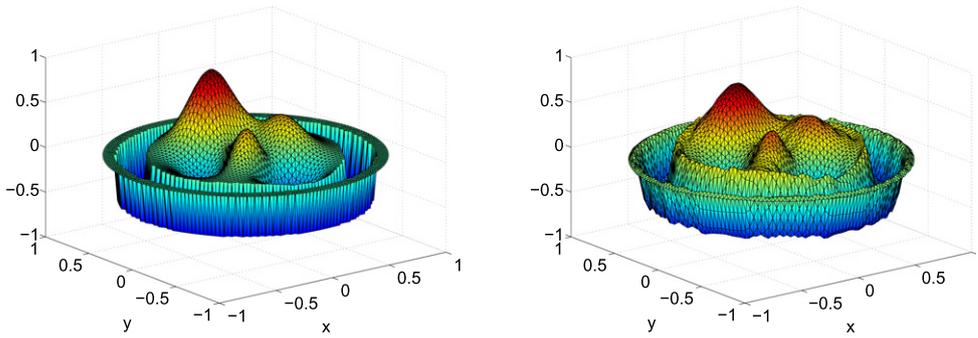
Figure 4. The inverse source scattering problem: (left) exact current density source function; (right) reconstructed current density source function.

Although the uniqueness and stability results are established for the homogeneous medium, the numerical method, i.e., the continuation method, works for the inhomogeneous medium. In the numerical example below, we take the scatterer function as the example q defined in section 2.6.

To demonstrate the effectiveness of the numerical method, let us consider a nonsmooth current density source function

$$f(x, y) = \begin{cases} \tilde{q}(4x, 4y) & \text{for } |\mathbf{r}| < 0.7 \\ -0.5 & \text{for } 0.7 \leqslant |\mathbf{r}| \leqslant 0.9 \\ 0.0 & \text{for } |\mathbf{r}| > 0.9 \end{cases}$$

inside the unit ball $B = \{\mathbf{r} \in \mathbb{R} : |\mathbf{r}| < 1\}$. The exact source function is plotted in figure 4 (left). By starting at $\kappa_{\min} = 1.0$, we adopt the above continuation algorithm with equally spaced wavenumbers $\Delta\kappa = 1.0$, and stop at $\kappa_{\max} = 61.0$. Only one Landweber iteration is applied at each fixed wavenumber κ_j. The step length parameter is taken as $\alpha_j = \kappa_j^2$. The final reconstructed source is shown in figure 4 (right). It can be observed that the reconstructed solution captures both the macro structures and the small scales of the source, and the source function is accurately reconstructed with multiple frequency data. To demonstrate the convergence of the method, figure 5 plots the evolution of the reconstructed solutions at various wavenumbers.

4. Discussions and future works

The inverse scattering problems are studied in the present paper for the acoustic wave propagation in two dimensions. In order to overcome the instability of the problems at a fixed frequency, the stable multi-frequency data based RLM is introduced. It is proceeded by recursively solving the direct and adjoint problems at higher wavenumbers, not only a better approximation but also a finer resolution can be achieved. The method is shown mathematically and numerically for being stable and effective to solve the inverse scattering problems with increased resolution. In particular, the stability estimate of the ISP indicates that it is linear to recover the source function with respect to the noise for large wavenumbers. However, it is completely open for the stability estimate of the nonlinear IMP and remains the subject matter of much ongoing research. In the extreme case of all frequencies, the relevant estimates have been obtained in [33, 34].
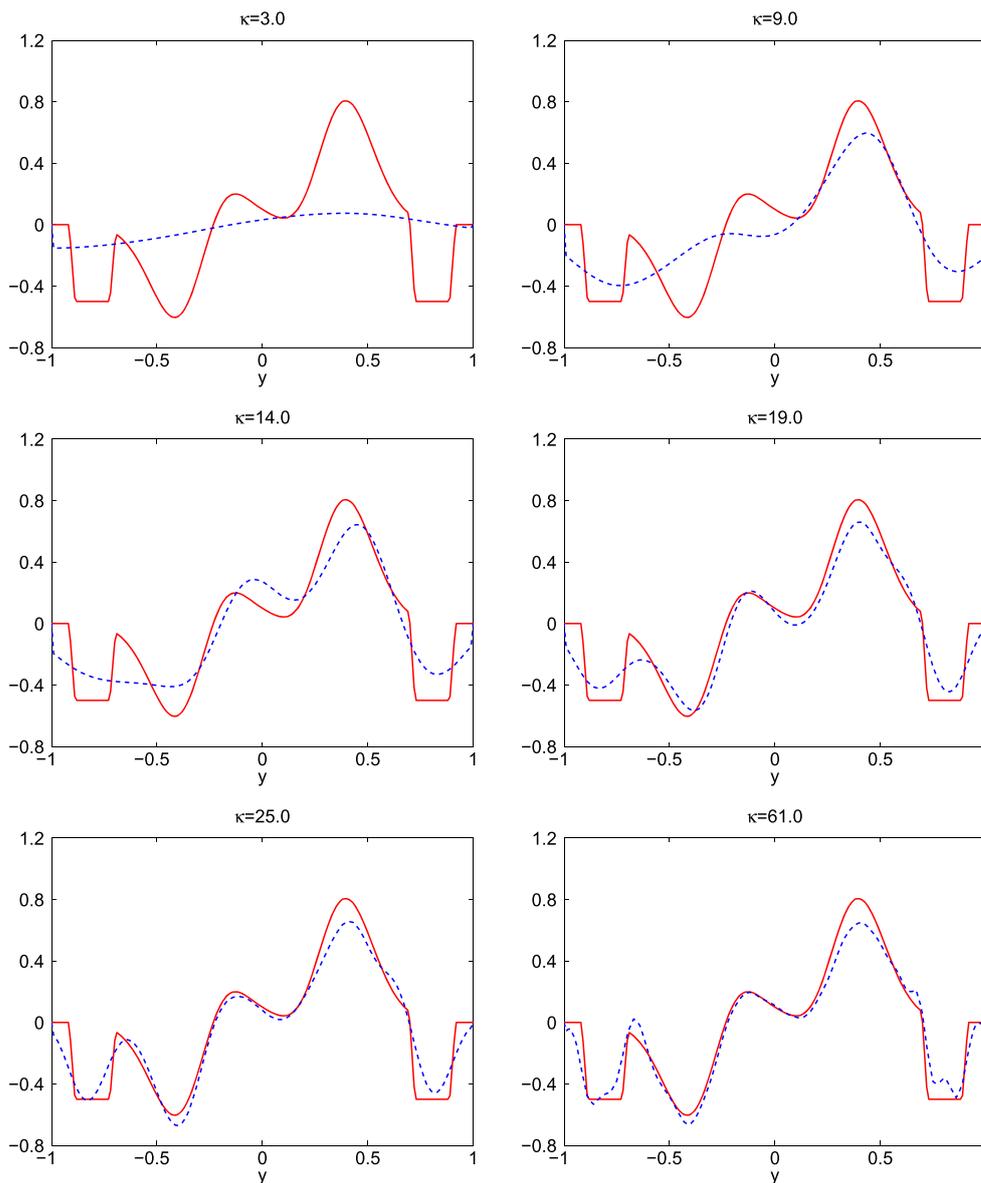
Figure 5. The reconstructed current density source function (dashed line) is plotted against the exact current density source function (solid line) for the cross-section $x = 0$.

We point out some future directions along the line of this research. It is challenging to solve the inverse scattering problems with incomplete or phaseless data. These problems become even more ill-posed without full information of the data. Some preliminary work has been done in [20] for solving the inverse diffraction grating problem with phaseless data. The present paper only addresses the deterministic inverse scattering problems, i.e., the scatterer and the current density source are all represented by deterministic functions. It is worthwhile to investigate the stochastic inverse scattering problems, which refer to the inverse scattering

problems involving uncertainties. Compared to deterministic counterparts, stochastic inverse scattering problems have substantially more difficulties on top of the existing hurdles due to the randomness and uncertainties. The scatterer function q and the source function f should be modeled as random functions for the inverse random medium scattering problem and the inverse source scattering problem, respectively. Initial effort has been made for solving inverse random source scattering problem of the one-dimensional Helmholtz equation [11, 88]. It is not clear how to extend the method to the higher dimensional Helmholtz equation and Maxwell equations. It is of a broad interest to consider the more challenging inverse random medium scattering problem. The medium is no longer deterministic and its randomness and uncertainty have to be modeled as well. Another significant problem is the imaging of objects with a shape that has multiple scales. For a multi-scale surface localized on a ground plane, a continuation procedure is proposed in [23] to reconstruct the large scale features at low frequencies and capture small scales of the surface at higher frequencies. A promising technique is to combine the RLM and near-field imaging methods to obtain the full image of the multiple scale objects in an efficient way. It is a hot and challenging topic on super resolution in inverse scattering problems [6]. The research of inverse scattering problems lies at the interface of mathematics, physics, engineering, and materials sciences. It will contribute towards better understandings of the complex physical and mathematical problems in scattering theory of optics and electromagnetics. We hope to be able to report the progress on these aspects elsewhere in the future.

Acknowledgments

References

[1] Amundsen L, Reitan A, Helgesen H and Arntsen B 2005 Data-driven inversion/depth imaging derived from approximation to one-dimensional inverse acoustic scattering *Inverse Problems* **21** 1823–50

[2] Albanese R and Monk P 2006 The inverse source problem for Maxwell's equations *Inverse Problems* **22** 1023–35

[3] Ammari H, Bahouri H, dos Santos Ferreira D and Gallagher I 2013 Stability estimates for an inverse scattering problem at high frequencies *J. Math. Anal. Appl.* **400** 525–40

[4] Ammari H and Bao G 2001 Analysis of the scattering map of a linearized inverse medium problem for electromagnetic waves *Inverse Problems* **17** 219–34

[5] Ammari H, Bao G and Fleming J 2002 An inverse source problem for Maxwell's equations in magnetoencephalography *SIAM J. Appl. Math.* **62** 1369–82

[6] Ammari H and Zhang H 2015 Super-resolution in high contrast media *Proc. R. Soc.* A **471** 20140946

[7] Angel T, Kirsch A and Kleinmann R 1991 Antenna control and generalized characteristic modes *Proc. IEEE* 79 1559–68

[8] Badia A and Nara T 2011 An inverse source problem for Helmholtz's equation from the Cauchy data with a single wave number *Inverse Problems* **27** 105001

[9] Badia A and Nara T 2013 Inverse dipole source problem for time-harmonic Maxwell equations: algebraic algorithm and Holder stability *Inverse Problems* **29** 015007

[10] Bao G, Chen Y and Ma F 2000 Regularity and stability for the scattering map of a linearized inverse medium problem *J. Math. Anal. Appl.* **247** 255–71
[11] Bao G, Chow S-N, Li P and Zhou H 2014 An inverse random source problem for the Helmholtz equation *Math. Comp.* **83** 215–33
[12] Bao G, Chow S-N, Li P and Zhou H 2010 Numerical solution of an inverse medium scattering problem with a stochastic source *Inverse Problems* **26** 074014
[13] Bao G, Hou S and Li P 2007 Inverse scattering by a continuation method with initial guesses from a direct imaging algorithm *J. Comput. Phys.* **227** 755–62
[14] Bao G and Li P 2004 Inverse medium scattering for three-dimensional time harmonic Maxwell's equations *Inverse Problems* **20** L1–7
[15] Bao G and Li P 2005 Inverse medium scattering problems for electromagnetic waves *SIAM J. Appl. Math.* **65** 2049–66
[16] Bao G and Li P 2007 Inverse medium scattering problems in near-field optics *J. Comp. Math.* **25** 252–65
[17] Bao G and Li P 2007 Numerical solution of inverse scattering for near-field optics *Opt. Lett.* **32** 1465–7
[18] Bao G and Li P 2005 Inverse medium scattering for the Helmholtz equation at fixed frequency *Inverse Problems* **21** 1621–41
[19] Bao G and Li P 2009 Numerical solution of an inverse medium scattering problem for Maxwell's equations at fixed frequency *J. Comput. Phys.* **228** 4638–48
[20] Bao G, Li P and Lv J 2013 Numerical solution of an inverse diffraction grating problem from phaseless data *J. Opt. Soc. Am.* A **30** 293–9
[21] Bao G, Li P and Wu H 2012 A computational inverse diffraction grating problem *J. Opt. Soc. Am.* A **29** 394–9
[22] Bao G and Lin J 2011 Imaging of local surface displacement on an infinite ground plane: the multiple frequency case *SIAM J. Appl. Math.* **71** 1733–52
[23] Bao G and Lin J 2012 Imaging of reflective surfaces by near-field optics *Opt. Lett.* **37** 5027–9
[24] Bao G, Lin J and Mefire S 2014 Numerical reconstruction of electromagnetic inclusions in three-dimensions *SIAM J. Imaging Sci.* **7** 558–77
[25] Bao G, Lin J and Triki F 2010 A multi-frequency inverse source problem *J. Differ. Equ.* **249** 3443–65
[26] Bao G, Lin J and Triki F 2011 Numerical solution of the inverse source problem for the Helmholtz equation with multiple frequency data *Contemp. Math.* **548** 45–60
[27] Bao G, Lin J and Triki F 2011 An inverse source problem with multiple frequency data *C. R. Math.* **349** 855–9
[28] Bao G and Liu J 2003 Numerical solution of inverse problems with multi-experimental limited aperture data *SIAM J. Sci. Comput.* **25** 1102–17
[29] Bao G, Lu S, Rundell W and Xu B 2015 A recursive algorithm for multi-frequency acoustic inverse source problems *SIAM J. Numer. Anal.* **53** 1608–28
[30] Bao G and Triki F 2010 Error estimates for the recursive linearization for solving inverse medium problems *J. Comput. Math.* **28** 725–44
[31] Bao G and Triki F 2013 Reconstruction of a defect in an open waveguide *Sci. China Math.* **56** 2539–48
[32] Bao G and Triki F Stability estimates for the 1d multifrequency inverse medium problem preprint
[33] Bao G and Yun K 2009 On the stability of an inverse problem for the wave equation *Inverse Problems* **25** 045003
[34] Bao G and Zhang H 2014 Sensitive analysis of an inverse problem for the wave equation with caustics *J. Am. Math. Soc.* **27** 953–81
[35] Bleistein N and Cohen J 1977 Nonuniqueness in the inverse source problem in acoustics and electromagnetics *J. Math. Phys.* **18** 194–201
[36] Burger M 2004 Levenberg–Marquardt level set methods for inverse obstacle problems *Inverse Problems* **20** 259–82
[37] Cakoni F and Colton D 2005 *Qualitative Methods in Inverse Scattering Theory: An Introduction* (Berlin: Springer)
[38] Carney S and Schotland J 2000 Inverse scattering for near-field microscopy *Appl. Phys. Lett.* **77** 2798–800
[39] Carney S and Schotland J 2001 Three-dimensional total internal reflection microscopy *Opt. Lett.* **26** 1072–4

[40] Carney S and Schotland J 2002 Determination of three-dimensional structure in photon scanning tunneling microscopy *J. Opt.* A **4** 140–4

[41] Carney S and Schotland J 2003 Theory of total-internal-reflection tomography *J. Opt. Soc. Am.* A **20** 542–7

[42] Carney S and Schotland J 2003 Near-field tomography *MSRI Ser. Math. Appl.* **47** 131–66

[43] Chen Y 1997 Inverse scattering via Heisenberg uncertainty principle *Inverse Problems* **13** 253–282

[44] Chen Y 1997 Inverse scattering via skin effect *Inverse Problems* **13** 649–67

[45] Chen Y and Rokhlin V 1997 On the Riccati equations for the scattering matrices in two-dimensions *Inverse Problems* **13** 1–13

[46] Cheney M 2001 The linear sampling method and the music algorithm *Inverse Problems* **17** 591–5

[47] Cheng J, Liu J-J and Nakamura G 2005 The numerical realization of the probe method for the inverse scattering problems from the near-field data *Inverse Problems* **21** 839–55

[48] Chew W and Wang Y 1990 Reconstruction of two-dimensional permittivity distribution using the distorted Born iteration method *IEEE Trans. Med. Imaging* **9** 218–25

[49] Coifman R, Goldberg M, Hrycak T, Israeli M and Rokhlin V 1999 An improved operator expansion algorithm for direct and inverse scattering computations *Waves Random Media* **9** 441–57

[50] Colton D, Coyle J and Monk P 2000 Recent development in inverse acoustic scattering theory *SIAM Rev.* **42** 369–414

[51] Colton D, Haddar H and Piana M 2003 The linear sampling method in inverse electromagnetic scattering theory *Inverse problems* **19** 105–37

[52] Colton D and Kirsch A 1996 A simple method for solving inverse scattering problems in the resonance region *Inverse Problems* **12** 383–93

[53] Colton D and Kress R 1983 *Integral Equation Methods in Scattering Theory* (New York: Wiley)

[54] Colton D and Kress R 1998 *Inverse Acoustic and Electromagnetic Scattering Theory* (Berlin: Springer)

[55] Courjon D 2003 *Near-field Microscopy and Near-field Optics* (London: Imperial College Press)

[56] Courjon D and Bainier C 1994 Near field microscopy and near field optics *Rep. Prog. Phys.* **57** 989–1028

[57] Devaney A 1979 The inverse problem for random sources *J. Math. Phys.* **20** 1687–91

[58] Devaney A, Marengo E and Li M 2007 The inverse source problem in nonhomogeneous background media *SIAM J. Appl. Math.* **67** 1353–78

[59] Devaney A and Sherman G 1982 Nonuniqueness in inverse source and scattering problems *IEEE Trans. Antennas Propag.* **30** 1034–7

[60] Dorn O, Bertete-Aguirre H, Berrymann J and Papanicolaou G 1999 A nonlinear inversion method for 3D electromagnetic imaging using adjoint fields *Inverse Problems* **15** 1523–58

[61] Dorn O, Miller E and Rappaport C 2000 A shape reconstruction method for electromagnetic tomography using adjoint fields and level sets *Inverse Problems* **16** 1119–56

[62] Eller M and Valdivia N 2009 Acoustic source identification using multiple frequency information *Inverse Problems* **25** 115005

[63] Engl H, Hanke M and Neubauer A 1996 *Regularization of Inverse Problems* (Dordrecht: Kluwer)

[64] Erhard K and Potthast R 2006 A numerical study of the probe method *SIAM J. Sci. Comput.* **28** 1597–612

[65] Fokas A, Kurylev Y and Marinakis V 2004 The unique determination of neuronal currents in the brain via magnetoencephalogrphy *Inverse Problems* **20** 1067–82

[66] Gelfand I M and Levitan B M 1955 On the determination of a differential equation from its spectral functions *Am. Math. Soc. Transl. Ser.* 2 **1** 253–304

[67] Girard C and Dereux A 1996 Near-field optics theories *Rep. Prog. Phys.* **59** 657–99

[68] Gruber F, Marengo E and Devaney A 2004 Time-reversal imaging with multiple signal classification considering multiple scattering between the targets *J. Acoust. Soc. Am.* **115** 3042–7

[69] Haddar H and Monk P 2002 The linear sampling method for solving the electromagnetic inverse medium problem *Inverse Problems* **18** 891–906

[70] Hähner P and Hohage T 2001 New stability estimates for the inverse acoustic inhomogeneous a medium problem and applications *SIAM J. Math. Anal.* **62** 670–85

[71] Hauer K, Kühn L and Potthast R 2005 On uniqueness and non-uniqueness for current reconstruction from magnetic fields *Inverse Problems* **21** 955–67

[72] He S and Romanov V 1998 Identification of dipole equations *Wave Motion* **28** 25–44
[73] Hettlich F 1995 Frechét derivatives in inverse obstacle scattering *Inverse Problems* **11** 371–82
[74] Hohage T 2001 On the numerical solution solution of a three-dimensional inverse medium scattering problem *Inverse Problems* **17** 1743–63
[75] Hohage T 2006 Fast numerical solution of the electromagnetic medium scattering problem and applications to the inverse problem *J. Comput. Phys.* **214** 224–38
[76] Hou S, Sølna K and Zhao H 2004 Imaging of location and geometry for extended targets using the response matrix *J. Comput. Phys.* **199** 317–38
[77] Hou S, Sølna K and Zhao H 2006 A direct imaging algorithm for extended targets *Inverse Problems* **22** 1151–78
[78] Hou S, Sølna K and Zhao H 2007 A direct imaging algorithm using far-field data *Inverse Problems* **23** 1533–46
[79] Ikehata M 1998 Reconstruction of an obstacle from the scattering amplitude at a fixed frequency *Inverse Problems* **14** 949–54
[80] Ikehata M 1999 Reconstruction of obstacle from boundary measurements *Wave Motion* **30** 205–23
[81] Isakov V 1989 Inverse source problems *Mathematics Surveys Monographs* vol 34 (Providence, RI: American Mathematical Society)
[82] Kirsch A 2002 The music algorithm and the factorization method in inverse scattering theory for inhomogeneous media *Inverse Problems* **18** 1025–40
[83] Kirsch A and Grinberg N 2008 *The Factorization Method for Inverse Problems* (Oxford: Oxford University Press)
[84] Kress R 2003 Newtons method for inverse obstacle scattering meets the method of least squares *Inverse Problems* **19** 91–104
[85] Kress R and Rundell W 1994 A quasi-Newton method in inverse obstacle scattering *Inverse Problems* **10** 1145–57
[86] Kress R and Rundell W 1999 Inverse obstacle scattering using reduced data *SIAM J. Appl. Math.* **59** 442–54
[87] Lax P D and Phillips R S 1967 *Scattering Theory* (New York: Academic)
[88] Li P 2011 An inverse random source scattering problem in inhomogeneous media *Inverse Problems* **27** 035004
[89] Natterer F 1986 *The Mathematics of Computerized Tomography* (Stuttgart: Teubner)
[90] Natterer F and Wübbeling F 1995 A propagation-backpropagation method for ultrasound tomography *Inverse Problems* **11** 1225–32
[91] Natterer F and Wübbeling F 2005 Marching schemes for inverse acoustic scattering problems *Numer. Math.* **100** 697–710
[92] Nédélec J-C 2000 *Acoustic and Electromagnetic Equations: Integral Representations for Harmonic Problems* (New York: Springer)
[93] Potthast R 2004 A new non-iterative singular sources method for the reconstruction of piecewise constant media *Numer. Math.* **98** 703–30
[94] Santosa F 1996 A level-set approach for inverse problems involving obstacles *ESAIM: Control Optim. Calculus Variations* **1** 17–33
[95] Sini M and Thanh N 2012 Inverse acoustic obstacle scattering problems using multifrequency measurements *Inverse Problems Imaging* **6** 749–73
[96] Schmidt R 1986 Multiple emitter location and signal parameter estimation *IEEE Trans. Antennas Propag.* **34** 276–80
[97] Stefanov P and Uhlmann G 1998 Stability estimates for the hyperbolic Dirichlet to Neumann map in anisotropic media *J. Funct. Anal.* **154** 330–58
[98] Stefanov P and Uhlmann G 2005 Boundary rigidity and stability for generic simple metrics *J. Am. Math. Soc.* **18** 975–1003
[99] Sun J, Carney S and Schotland J 2007 Strong tip effects in near-field optical tomography *J. Appl. Phys.* **102** 103103
[100] The Nobel Prize in Chemistry 2014 (http://nobelprize.org/nobel-prizes/chemistry/laureates/2014/)
[101] Vögeler M 2003 Reconstruction of the three-dimensional refractive index in electromagnetic scattering by using a propagating-backpropagation method *Inverse Problems* **19** 739–53
[102] Weglein A, Araújo F, Carvalho P, Stolt R, Matson K, Coates R, Corrigan D, Foster D, Shaw S and Zhang H 2003 Inverse scattering series and seismic exploration *Inverse Problems* **19** R27–83